Tectonics

Supporting Information 3 for:

Meso–Cenozoic geodynamic evolution of the Patagonian foreland: insights from low-temperature thermochronology in the Deseado Massif

Alexis Derycke[1,2], Marie Genge*[3,4,5], Cécile Gautheron[1], Massimiliano Zattin[3], Stefano Mazzoli[6], Cesar Witt[4], Hermann Zeyen[1], Rosella Pinna-Jamme[1], Frederic Haurine[1], Marcelo Márquez[7]

1 – Université Paris-Saclay, CNRS, GEOPS, 91405, Orsay, France

2 – Géosciences Rennes, UMR6118, CNRS Université de Rennes, France

3 – Department of Geosciences, University of Padua, Italy

4 – Université de Lille, CNRS, Université du Littoral—Côte d'Opale, UMR 8187, LOG, Laboratoire d'Océanologie et de Géosciences, F 59000 Lille, France

5 – Department of Earth Sciences, University of Hong Kong, Pokfulam Road, Hong Kong, SAR, China

6 – School of Science and Technology, Geology Division, University of Camerino, Italy

7 – Departimento de Geología, Universidad Nacional de la Patagonia SJB, Comodoro Rivadavia, Argentina

Table of content:

Thermal modelling results

<u>Model #1:</u>

At equilibrium, this model consists of a 400-meter column of air resting on a 1-kilometer homogeneous rock pile. To simulate the emplacement of a flow, a defined thickness of material (such as ignimbrite) at a specific temperature is placed in substitution for the air. After the emplacement of the flow, thermal relaxation calculations are conducted over a total duration of 10,000 years. Figure S9 presents all the characteristics of this model.

The time increments for the calculations are set at six months, and the distance increments are one meter. This choice was made after several tests demonstrated that the "instantaneous" warming (from 1 second to 1 month) produced by the flow only propagates a very short distance (less than 1 meter). This is attributed to the low thermal conductivity of the rocks.

To illustrate all scenarios, several simulations were conducted with the following parameters:

- Flow thicknesses of 100 meters and 200 meters
- Flow temperatures of 600°C and 1000°C for extreme cases

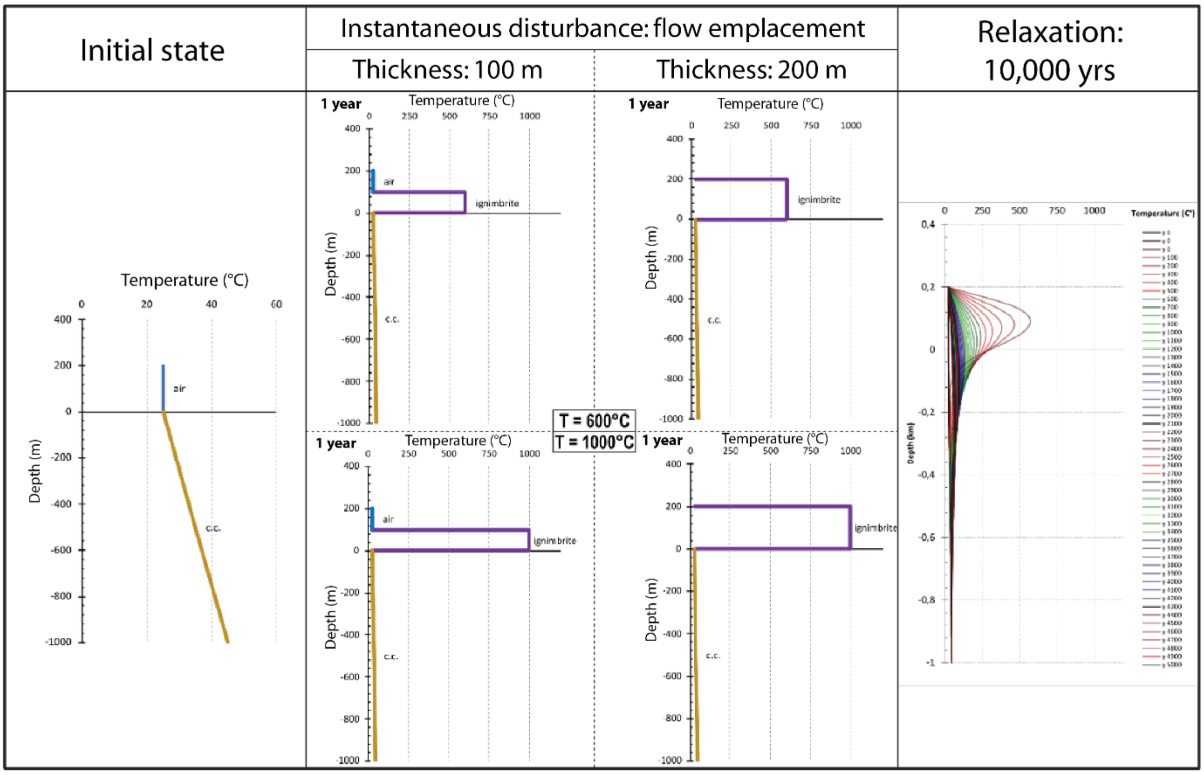

Figure S9: Model #1 to simulate the impact of a volcanic flow on the subsurface, simulations conducted using CAGES2D.

Figure S10 presents the temperature evolution over the first 500 years at depths of 0 m (in direct contact with the flow), 1 m, 10 m, and 100 m. The results indicate that the duration and amplitude of warming directly depend on the flow thickness, while the maximum temperature is influenced by the flow's temperature.

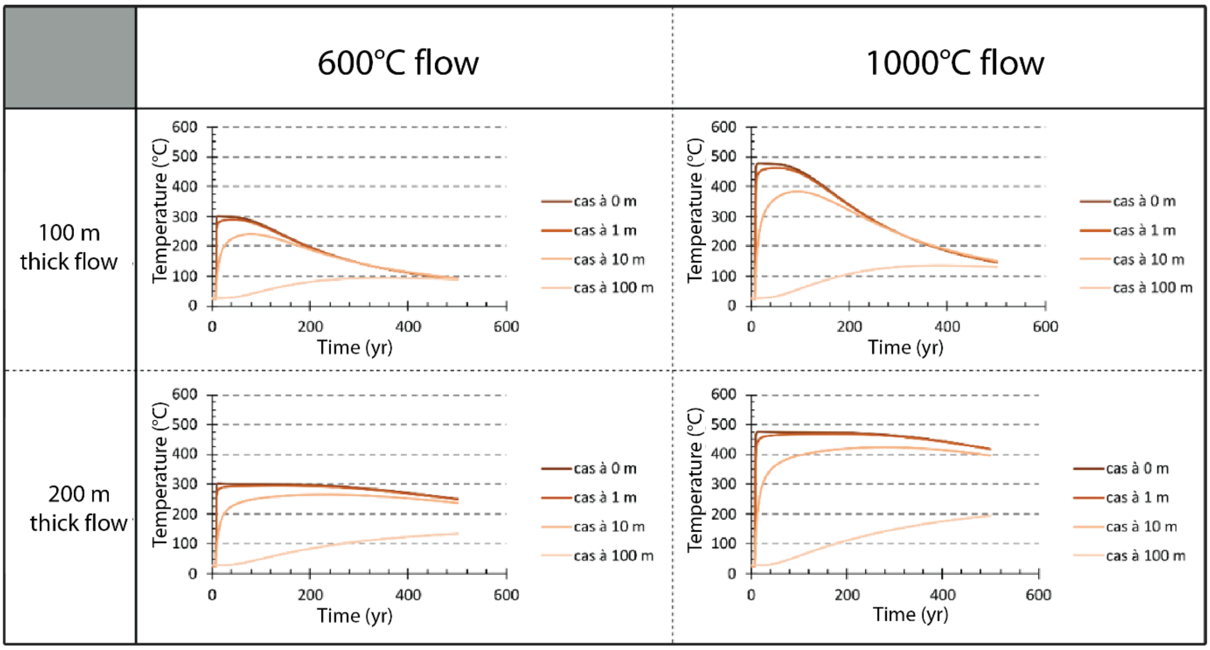

Figure S10: Temperature evolution over 500 years as a function of depth from 0 to 100 meters in the case of Model #1.

Figure S11 shows the temperature evolutions for the two extreme cases over 6,000 years, the time required for all depths to return to temperatures below 50°C in the extreme case of 1,000°C and 200 m thickness.

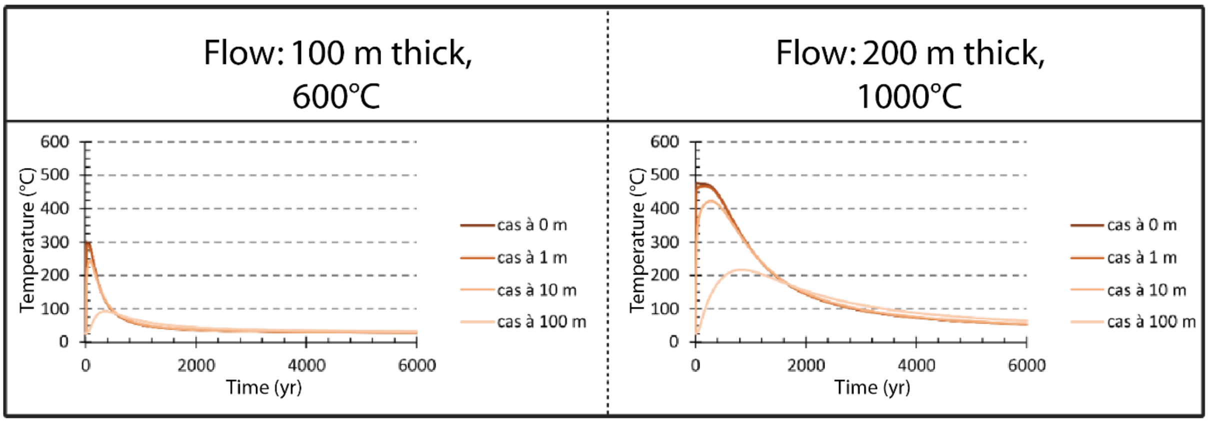

Figure S11: Evolution of temperature over 6,000 years as a function of depth from 0 to 100 meters in the case of Model #1.

After obtaining the temperature curves over time, as presented in Figures S10 and S11, it is possible to extract the durations for which samples at various depths were heated. These warming amplitudes (time-temperature) can then be displayed in an Arrhenius diagram, as shown in Figure S12, to compare their impacts on different thermochronometers. In this figure, only the distances of 1 m and 100 m below the flow are displayed, while the intermediate values represent a continuum between these two points.

For fission tracks in apatite, it is possible to quantify the shortening rate (r) of the fission tracks using Ketcham's healing model (2007). Figure S12 presents diagrams of the various flow envelopes along with the different iso-healing curves (iso-r) for apatites, with lengths of approximately 15 µm, 13.5 µm, and 9 µm (the latter corresponding to complete healing) for apatites. Using Ketcham's healing model (2007), it is possible to calculate associated track lengths for apatites that are weakly resistant to healing (rmr–0 = 0.8, Ketcham et al., 2007), which would correspond to lengths of approximately 14 µm and 11 µm, respectively. These results show that samples located within a few meters of a flow (< 10 m) will be partially to significantly healed by the heat generated (depending on their resistances). However, at distances of around one hundred meters, the impact becomes negligible, especially in the case of flows with temperatures of 600°C, which is close to the temperature of the flows.

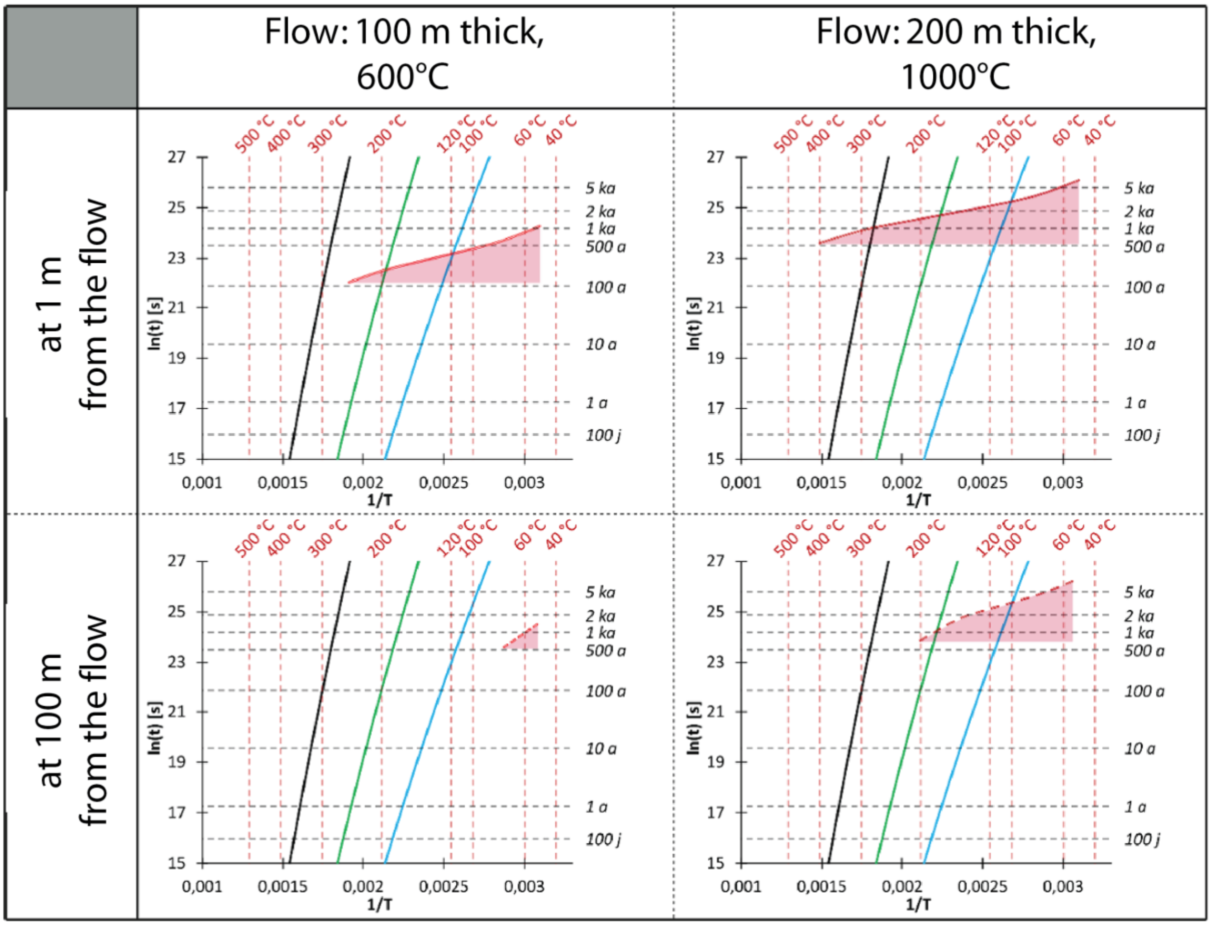

Figure S12: Arrhenius diagrams including the time-temperature warming envelopes achieved by the different morphologies of Model #1, as well as the iso-healing curves for fission tracks in apatite following Ketcham's model (2007): ***black curve****: rmr = 0.55 (~9 µm), corresponding to complete healing (Ketcham et al., 2007);* ***green curve****: rmr = 0.837 (~13.7 µm), corresponding to partial healing;* ***blue curve****: rmr = 0.937 (~15.1 µm), corresponding to stable healing at room temperature.*

In the case of (U-Th)/He, comparison is possible by including the iso-release rate curves in the same Arrhenius diagram. However, as presented in Figure S13, the models for helium diffusion in apatite are numerous and include several variable parameters. Therefore, it is essential to consider these parameters when evaluating the sensitivity to heating from a flow. As previously discussed in this study, the diffusion model of Gerin (2017) is preferred, and the iso-release rate lines from this model are presented in Figure S13. Additionally, Figure S13 shows the warming envelopes grouped into several graphs corresponding to varying damage values and activation energies. The results indicate the same trend as the fission track data: a negligible impact of flow heating at distances of around one hundred meters. However, the flow has a stronger influence, leading to total release for samples located within 1 meter (except for grains with high ΔEa). It is important to note that the (U-Th)/He system in apatite exhibits slight diffusion (less than 5%) at low temperatures, which explains the position of the 0% release curve.

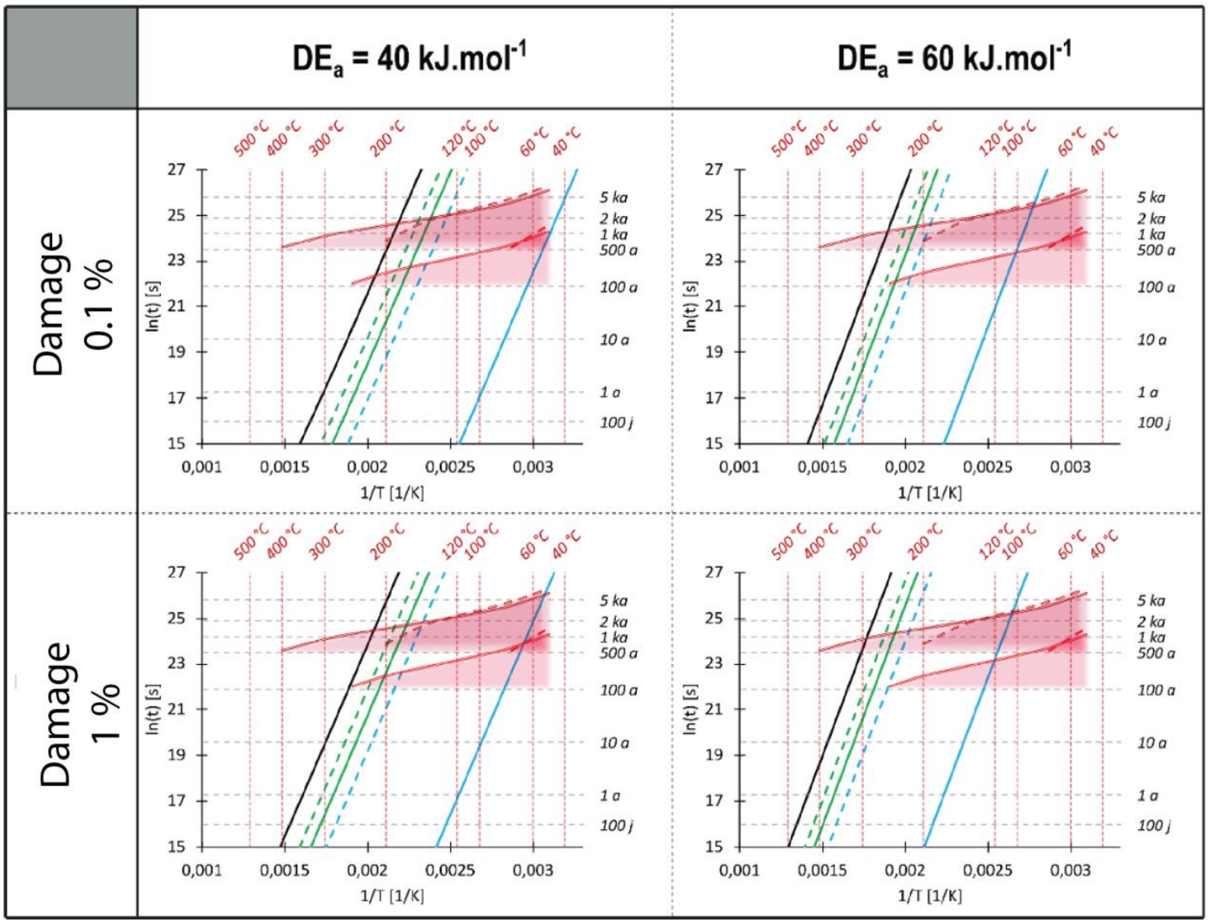

Figure S13: Arrhenius diagrams include the time-temperature envelopes achieved by the different morphologies of Model #1, as well as the helium iso-release lines in apatite following the Gerin model (2017): ***black line****: ~100% release; d***ashed green line****: 75% release.*

Model #2:

This model was constructed to evaluate the potential increase in the thermal gradient beneath the Deseado Massif caused by the complex mantle dynamics that existed between 210 and 140 Ma. To recap, this dynamics corresponds to the establishment of a flat slab, followed by the arrival of the debated Karoo-Ferrar plume. These events may have led to changes in the geothermal profile of the crust and could have influenced the thermal history of the samples.

To model the establishment of a flat slab and the arrival of a plume, it is necessary to base the model on a large-scale physical framework (approximately 200 km deep) and a long temporal scale (100 to 200 Ma). Since there is no bibliographic data on the structure of the crust and mantle beneath the Deseado Massif, the initial state of the model corresponds to a continental crust of 40 km thickness resting on a continental lithosphere of 70 km. For the various modeling steps, the asthenosphere has also been modeled down to a depth of 200 km. Boundary conditions are set at 25°C at the surface and 1400°C at 200 km depth, with the parameters for the different materials referenced in Annex 6. To verify the validity of the initial state, temperatures at the asthenosphere-lithosphere and crust-mantle interfaces were calculated, corresponding to approximately 1350°C and 650°C, respectively, which align with expected temperatures.

The model is then modified according to the following steps:

1. **Establishment of the Flat Slab (5 to 25 Ma)**: Replacement of the asthenospheric mantle between 110 and 120 km with oceanic crust, and between 120 and 160 km with oceanic lithosphere.
2. **Withdrawal of the Slab and Arrival of the Hotspot (25 to 30 Ma)**: Replacement of materials between 110 and 200 km with mantle material, with temperatures at the interfaces ranging from 1800°C (200 km) to 1450°C (110 km). The subcontinental lithosphere is replaced by a more hydrated lithosphere.
3. **Existence of the hotspot (30 to 70 Ma)**, referred to as the "hotspot phase": the asthenosphere-lithosphere boundary rises to 90 km, with an elevated asthenospheric temperature of 1800°C at the base.
4. **Relaxation (70 to 200 Ma)**: the temperature of the asthenosphere returns to "normal" values (1400°C).

Initially, the modeling was conducted considering a model without accounting for vertical movement (isostatic dynamics) to determine the consequences of heat transfer by diffusion within the crust.

Subsequently, the same modeling was tested by incorporating a simple vertical dynamic, specifically based on isostatic equilibrium, to quantify thermal transfer by advection. Figure S14 shows the temperature changes at subsurface levels (1, 2.5, and 5 km deep) and at the crust-mantle interface located at 40 km depth. These results indicate a slight delay in temperature increase compared to the arrival and "life" of the plume, with a gradual rise of 300°C at the base of the crust and an increase of less than 25°C at subsurface levels. The results of this modeling demonstrate that in a simplified case, the flat slab-plume mantle dynamics do not produce significant temperature changes at the subsurface level. Thus, samples located at depths of less than 5 km experience a warming of less than 20°C, and even less than 10°C at depths below 2.5 km in this context.

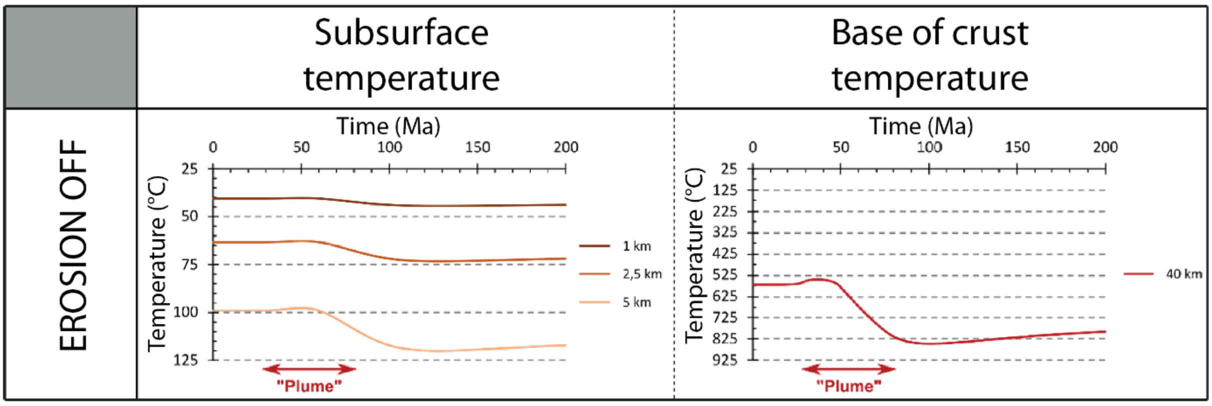

Figure S14: Temperature evolution over 200 Ma, at subsurface levels and at the base of the crust, for Model #2 (without vertical dynamics).

Figure S15 presents the results of the modeling that incorporates the isostatic equilibrium of the crust, as well as a simple erosion model based on altitude. The first set of results in Figure S14 shows the temperature changes over time for nodes at a "comparable" depth to that of the previous model, along with the temperature evolution at the crust-lithosphere interface (~40 km). The second set of results illustrates the depth evolution of these nodes over time, as well as the changes in topography and cumulative erosion over the 200 Ma of the model. The rapid cooling of subsurface nodes, visible between 0 and 30 Ma, corresponds to advection/exhumation of the nodes in response to the isostatic-erosional dynamics of the crust during the establishment of the flat slab. This response is characterized by a total erosion of approximately 10 km of the crust. Following this advection/erosion, the nodes located between 5 and 10 km depth show a warming of about ten degrees, corresponding to the arrival of the temperature wave from the plume. Simultaneously, the model stabilizes with a topography of 500 to 1000 meters and a relatively constant erosion rate. While the values for topography and erosion are not quantitative, it is notable that the establishment of a flat slab leads to a significant isostatic imbalance, whereas the model remains "stable" afterward.

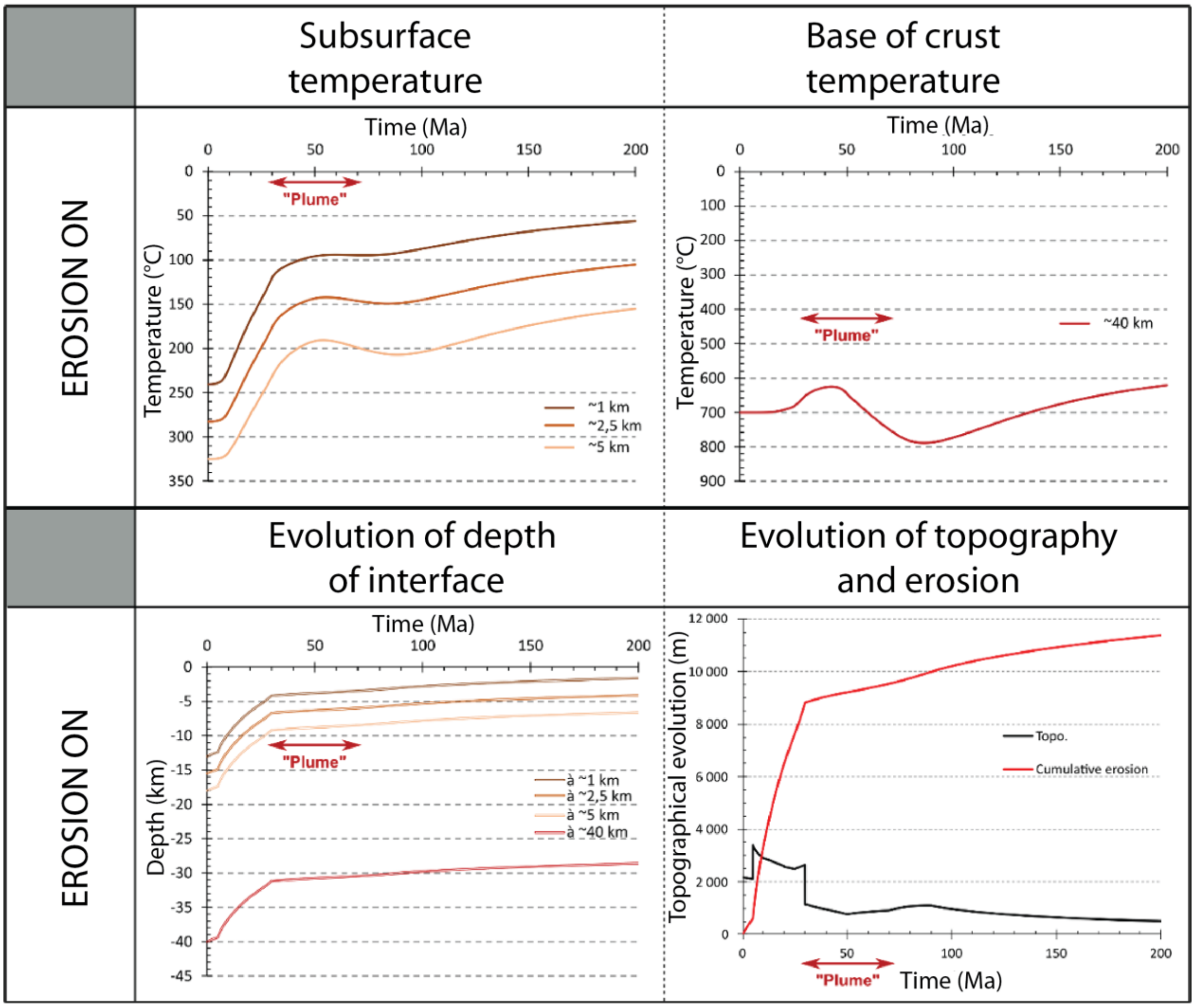

Figure S15: Results of Model #2 (with vertical dynamics): Temperature evolution over time (200 Ma) for nodes terminating in the subsurface and located at the base of the crust (~40 km) in the case of model number 2 (with vertical dynamics). Evolution of node depth, topography, and erosion over time (200 Ma) in the case of Model #2.

Model #3:

After assessing the impact of a lava flow on surface samples (less than a hundred meters) and the effect of mantle dynamics on the overall thermal profile, it is relevant to test the combined impact of these two phenomena, as well as the effect of burial under multiple flows. To evaluate these effects, the temperature evolution at the base of the crust from the previous model has been extracted and used as a constraint for the base of the crust to simply model the arrival of the hotspot. In addition to this constraint, the deposition method from model number 1 is used to simulate gradual burial under different materials.

This "deposition-plume" model lies at the boundary between the two previous models. In this case, a continental crust of 40 km thickness, topped by a 3 km air column, is modeled. At the base of the crust, successive volcanic deposits ranging from 100 to 200 m in thickness are added at a fixed interval of 10,000 years, totaling 2 km in thickness. In parallel with these deposits, the temperature at the base of the crust evolves according to the parameters from the previously modeled plume, over a period of 25 Ma. To compare the impact of hot deposits (such as CVBL) and colder deposits (like Cretaceous sediment cover), simulations were conducted with different deposit temperatures: 600°C, 1000°C, and 10°C. The 10 ka interval between each deposit was chosen to reflect a volcanic eruption cyclicity and to test the potential cumulative effect of hot material deposition. As demonstrated by model number 1, a flow that cools completely in less than ~10 ka would not produce any cumulative temperature effects with a slower cyclicity (e.g., 50 ka). The case of depositing cold materials implies a sedimentary rather than volcanic origin for the materials. However, the deposition dynamics used in this model, with 100 to 200 m every 10 ka, corresponds to a sedimentation rate of 10 to 20 km/Ma. Such a sedimentation rate is unrealistic in nature, but in order to compare equivalent models, the same deposition dynamics is maintained for the "cold deposit" simulations.

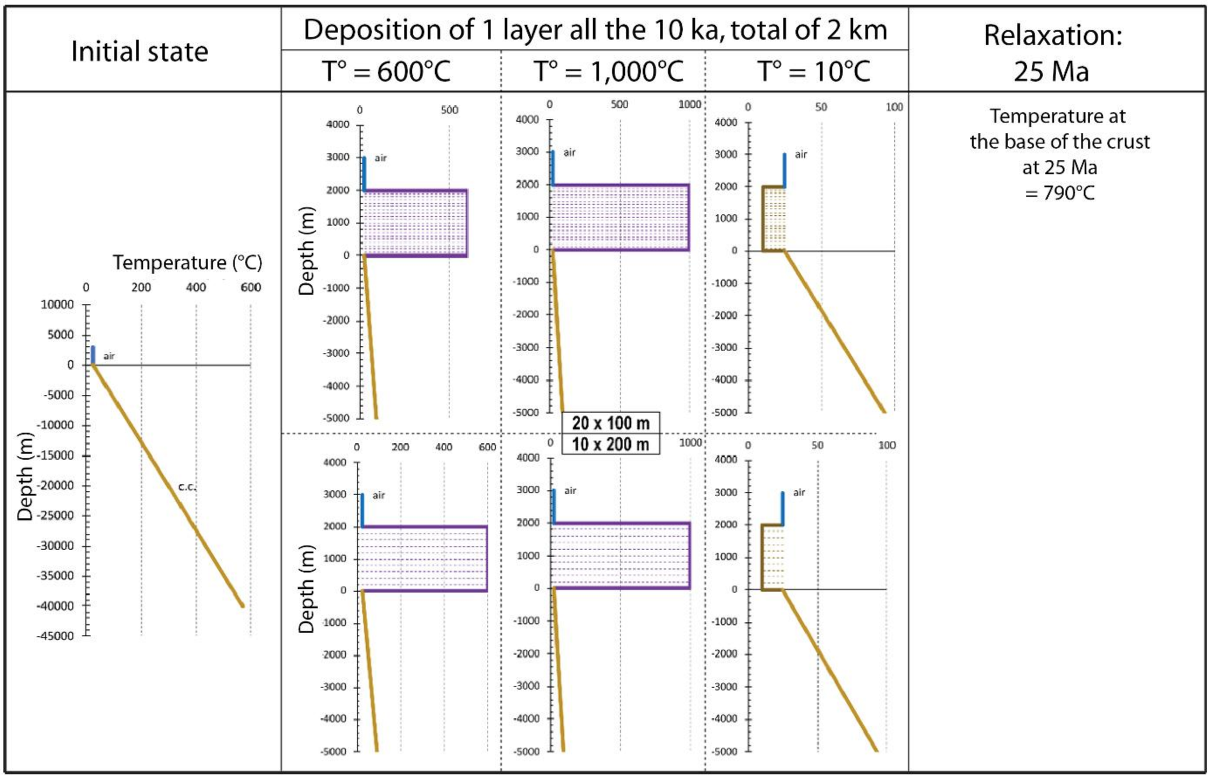

Figure S16: Model #3, which allows for modeling the impact of burial under material (hot and cold) and the change in thermal gradient in the subsurface, with simulations conducted using CAGES 1.5D.

The first expected result, but not presented here, corresponds to the decoupling between the impact of hot deposits and the modification of the thermal gradient by a plume. Indeed, as discussed previously, the establishment of hot deposits disrupts the system on a timescale of less than 10 ka, while the propagation of the heat wave from the arrival of a plume through the crust spans tens of Ma. The significant difference in the speed of these two processes prevents a cumulative effect; thus, whether the burial occurs under hot or cold deposits does not alter the modification of the thermal gradient caused by the plume. Figures 17 and 18 present the results of the temperature evolution for nodes located at depths of 100 m, 1 km, 2.5 km, and 5 km beneath the flow, in order to constrain the impact of burial on subsurface samples before the onset of deposits. Figure S16 compares the results of hot and cold deposits, highlighting the differences between the two types of deposits.

The first difference lies in the time required to reach the "equilibrium" burial temperature; specifically, it takes 1 Ma and 0.5 Ma for cold and hot deposits, respectively. This difference is explained by the heat contribution from hot deposits, which accelerates the equilibration process. The second difference corresponds to the temperature increase produced by the establishment of hot deposits. Indeed, the presence of hot deposits raises the temperature of the rocks beneath them above the equilibrium temperature up to about 1 km; their influence is observable down to 2.5 km, where the temperature increases more rapidly than that of cold deposits but remains below the equilibrium temperature.

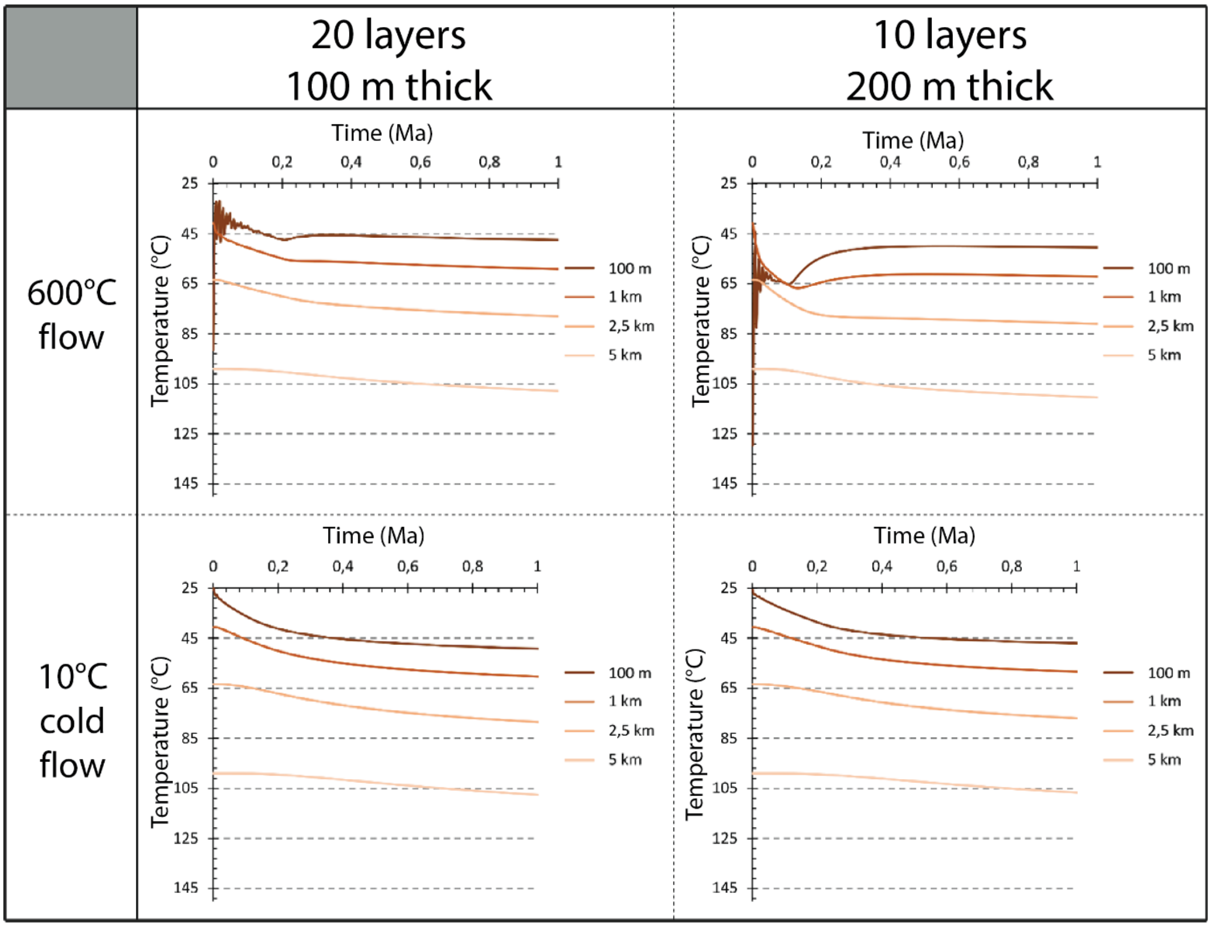

Figure S17: Evolution of temperature over time for 1 Ma in the subsurface, in the case of model #3.

Figure S18 provides a more detailed view of the first 0.5 million years in the case of hot deposits at 600 °C and 1000 °C. These results highlight that, with a similar deposition dynamic (e.g., 20 flows of

100 meters) but at different temperatures (600 °C vs. 1000 °C), the thermal evolution dynamics are similar, with only the amplitude of warming changing. In the case of 100-meter thick layers, a cumulative effect is observed down to more than 100 m in depth, with a significant temperature increase during the first 100 thousand years. The temperatures reached are between 70 °C and 40 °C, placing this zone at temperatures higher than the equilibrium burial temperature (~40 °C). For 200-meter thick layers, the same phenomenon is observed but with significantly greater intensity. Indeed, the temperatures reached before 100 ka exceed equilibrium temperatures (more than 90-60 °C) and extend down to over 1 km in depth for flows at 1000 °C. Finally, in the case of 200 m thick flows, a "saturation" effect of warming appears at 100 m depth and at ~0.05 Ma (50 ka). This saturation effect corresponds to the moments when more than 1 km of deposits have formed, creating a thermal shield against the propagation of heat from the flows.

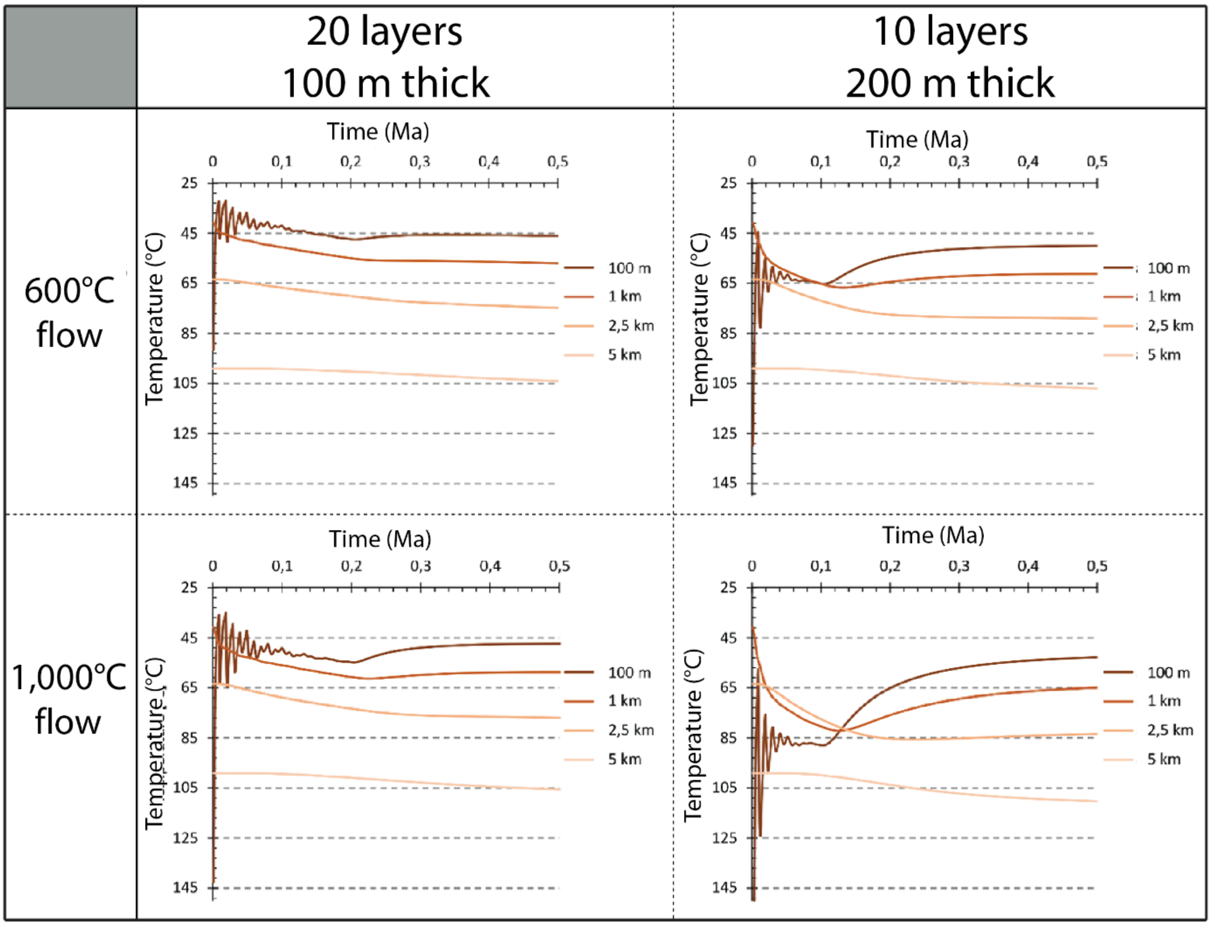

Figure S18: Evolution of temperature over time for 0.5 Ma in the subsurface, in the case of model number 3 with different configurations of hot deposits.

Firstly, this model demonstrates that there is no combined effect between the warming resulting from the arrival of a plume and that associated with the deposition of hot material at the surface. However, this statement is only true when the two events are temporally close; in the case of a thermal gradient increase before the establishment of hot deposits, a combined effect could exist. Next, model number 3 highlights a cumulative phenomenon produced during the deposition of several layers of hot material, which is a short-term effect (<100 ka) on geological timescales (>10 Ma). This results in a significant temperature increase over the first 100 meters of depth, detectable over the first kilometer, and negligible at greater depths. Additionally, the exact dynamics of temperature increase depend on the morphology of the deposits (e.g., recurrence, thickness, temperature, etc.). Finally, this phenomenon experiences a "saturation" effect when buried under more than approximately 1 km of material, with the temperature evolution then returning to that of burial under cold deposits.